Buildup and structure of the InSe/Pt interface studied by angle-resolved photoemission and x-ray absorption spectroscopy

J. F. Sánchez-Royo,[1,*] J. Pellicer-Porres,[1] A. Segura,[1] S. J. Gilliland,[1] J. Avila,[2,3] M. C. Asensio,[2,3] O. Safonova,[4] M. Izquierdo,[2] and A. Chevy[5]

[1]*ICMUV, Universidad de Valencia, c/Dr. Moliner 50, 46100 Burjassot, Valencia, Spain*

[2]*Synchrotron SOLEIL, L'Orme des Merisiers, Saint-Aubin Boîte Postal 48, 91192 Gif-sur-Yvette Cedex, France*

[3]*Instituto de Ciencia de Materiales de Madrid, CSIC, Cantoblanco, 28049 Madrid, Spain*

[4]*ESRF, Boîte Postal 220, F-38043 Grenoble Cedex, France*

[5]*Laboratoire de Physique des Milieux Condensés, Université Pierre et Marie Curie, 4 place Jussieu, 75252 Paris Cedex 05, France*

(Received 18 October 2005; revised manuscript received 5 January 2006; published 10 April 2006)

The atomic structure and the electronic nature of the InSe/Pt interface have been studied by x-ray absorption spectroscopy and angle-resolved photoemission, respectively. By these measurements, it has been found that Pt atoms equally incorporate into two trigonal-prismatic intralayer positions existing within the InSe layer, although, at low Pt coverage, Pt atoms seem to prefer one of these sites, where they have a lower interaction with Se atoms. The atomic structure of the InSe/Pt interface appears to determine its electronic behavior as Pt deposition increases. At initial stages of Pt diffusion, isolated Pt atoms act as a surface acceptor which turns the interface into intrinsic. Beyond a certain submonolayer Pt coverage, Pt-InSe reaction gives rise to localized states within the InSe band gap coming from the InSe valence band maximum. These states appear to mostly determine the InSe/Pt barrier height before the onset of metallization expected by the formation of a bulklike Pt layer. As a result, the atomic structure of the InSe/Pt interface has appeared to be quite far from that expected for an ideal InSe/Pt interface and the formation of a final bulk-like Pt layer scarcely contributes to the electron barrier height at the interface. Nevertheless, the final InSe/Pt barrier height appears to be that expected for an abrupt InSe/Pt Schottky interface.

DOI: 10.1103/PhysRevB.73.155308 PACS number(s): 79.60.Jv, 73.30.+y, 61.10.Ht

I. INTRODUCTION

The study of metal/semiconductor (or insulating) interfaces has been extensively performed for decades and, for clear technological reasons, is one of the most active areas in solid state physics. In spite of the large amount of systems studied, there is not a clear valid model yet for as basic aspects as the correlation between the structural nature and the electronic structure of the interface.[1] In the Schottky model of the interface no metal-semiconductor interaction is assumed, so charge accumulated at the interface comes from the free surfaces of the metal and semiconductor and its value depends on the metal work function and the semiconductor electron affinity. Nevertheless, the common existence of interface states at the semiconductor band gap breaks this scheme, giving rise to the pinning of the Fermi level (E_F) at the interface. Different mechanisms have been found to be responsible for the E_F pinning, such as metal induced gap states,[2,3] surface states,[4] or defect states.[5,6] The different nature of these mechanisms implicitly conveys a particular atomic arrangement of the interface. Therefore, a precise determination of the atomic structure and reactivity of the interface would be required in order to understand the electronic behavior of the interface,[7,8] tune them in a controlled manner,[9,10] and consequently open the possibility of designing new devices with particular conducting properties.[11,12]

In this context, the study of metal/semiconductor interfaces based on layered materials may contribute to clarify some of the above mentioned basic aspects in systems with important technological applications, due to their particular surface atomic structure. Since the development of the so-called van der Waals epitaxy,[13] III-VI layered semiconductors, such as GaSe, GaS, and InSe, are the object of a renewed interest due to the open possibilities of preparing high-quality systems with potential applications in nonlinear and optical bistable devices,[14,15] solar cells,[16,17] and solid-state batteries.[18,19] One of the advantages of this epitaxy mode, compared to standard molecular beam epitaxy ones, is that matching requirements of lattice parameter are relaxed by the fact that their (001) surfaces do not present any dangling bond and film-substrate cohesive mechanisms are driven by weak van der Waals forces. This particular nature of the van der Waals surfaces has allowed one to prepare abrupt layered-compound interfaces[17,20] and, moreover, it has been proposed to use GaS, GaSe, or InSe as buffer layers to grow thin films over substrates with a large lattice mismatch.[21,22]

As far as layered-compound epitaxy is concerned, these van der Waals surfaces have appeared to be, in principle, quite inert. Nevertheless, this precept has also been assumed for interfaces formed by deposition of other compounds or even metals. As a consequence, the problem of the nature of the interface has been frequently skipped and very few data can be found in the literature about the reactivity of these surfaces with deposited nonlayered compounds. Only a few reports have been published on III-VI semiconductors on the formation of Schottky barriers[23] (Au/InSe) or heterojunctions[24] (In_2O_3/InSe) but none of them addresses the subject of the interface structure. Among the interfaces formed by the addition of metallic atoms, the case of the

InSe/Pt interface is paradigmatic. In spite of the important role played by this barrier as a back surface field contact in 10% efficiency InSe-based solar cells,[16] the problem of the structure of this interface and the origin of the electronic barrier have not been approached up to now.

In this work we approach the study of the electronic nature of the barrier formed by deposition of Pt on *n*-InSe(001) surfaces, by angle-resolved photoemission measurements (ARPES) as well as the atomic structure of the InSe/Pt interface, by x-ray absorption spectroscopy (XAS). These techniques, combined with the use of synchrotron facilities, have demonstrated to be, by far, two of the most powerful tools for the characterization of thin films and heterostructures.[25] From the results obtained, the reactivity between deposited Pt and the InSe substrate has been analyzed, as well as the origin and formation of the InSe/Pt barrier at the interface. This paper is organized as follows. The experimental setup is described in Sec. II. In Sec. III, the experimental results obtained by XAS and ARPES are shown and discussed. Finally, in Sec. IV we present the main conclusions of this work.

II. EXPERIMENTAL

Part of the photoemission experiments were performed at LURE (Orsay, France) using the Spanish-French (PES2) experimental station of the Super-Aco storage ring, described elsewhere.[26] The measurements were carried out in a purpose-built ultrahigh-vacuum system, with a base pressure of 5×10^{-11} mbar, equipped with an angle resolving 50 mm hemispherical VSW analyzer coupled on a goniometer inside the chamber. The manipulator was mounted in a two-axes goniometer which allows rotation of the sample in the whole 360° azimuthal angle and in the 180° polar emission angle relative to surface normal (Θ), with an overall angular resolution of 0.5°. Photoelectrons were excited with *p*-polarized synchrotron radiation in the 18–150 eV energy range. For this selected photon energy ($h\nu$) range, the energy resolution varied from 60 meV ($h\nu<40$ eV) to 0.1 eV ($h\nu>80$ eV). With this setup, different energy-distribution curve (EDC) series were recorded scanning the $h\nu$ as well as Θ, at constant incident angle of the light of 45°. Under these conditions, polarization effects on initial states along one series are neglected. All the EDC spectra shown in this work refer to the E_F.

The *n*-type InSe single crystals used in this work (with a donor impurity concentration $N_d=10^{16}$ cm^{-3}) were cut from an ingot grown by the Bridgman-Stockbarger method. The samples were cleaved *in situ* after introduction in an ultrahigh vacuum chamber. The samples were easily cleaved in the layer plane due to the existence of weak interlayer van der Waals bonds. Low-energy electron diffraction (LEED) spectra showed a sharp spot pattern corresponding to the bulk rhombohedral material. No surface impurities were detected by photoemission measurements. The samples were oriented by azimuthal and polar photoelectron diffraction scans recording the Se 3*d* peak intensity. Platinum was evaporated from a tungsten filament with a deposition rate, as determined by a quartz microbalance, of 0.1 monolayers/min (ML/min). In this work, we have adopted that 1 ML equals 7.15×10^{14} atoms/cm^2, that is the InSe surface atomic density in the layer plane.

Samples for the XAS experiment were prepared with the same procedure described above, in an ultrahigh-vacuum evaporation chamber connected to an ESCALAB 210 multianalysis system (base pressure 1.0×10^{-10} mbar) from Thermo VG Scientific available in our laboratory. In the preparation of this set of samples, the amount of Pt deposited was controlled by the relative photoemission intensity between the Pt 4*f* and In 3*d* core levels, these excited by x-ray photoemission (XPS) with the Mg-$K\alpha$ line. A series of samples with a Pt coverage ranging from 0.4 to 4 ML was prepared. Each sample was cut into 4 pieces and 3 of them were annealed in high vacuum (10^{-7} mbar) at temperatures of 500, 600, and 700 K for 4 h. Samples had typical sizes of $4\times4\times0.01$ mm^3. All sample preparation was done during the two weeks just before the experiment. The fluorescence-detected XAS experiments were carried out at the ID26 beamline in the ESRF synchrotron. A Si (220) double-crystal monochromator was used for these experiments. Two Cr mirrors at 3.2 mrad were introduced to remove high-energy harmonics from the incident beam. The spectra were acquired at the Pt LIII absorption edge, by using a silicon diode placed perpendicular to the x-ray beam, in order to minimize elastically scattered radiation. For all experiments, a reference Pt foil was used to provide an internal and accurate energy calibration for all spectra (first inflection point 11564 eV). Except when explicitly stated, we employed grazing incidence, with the x-ray polarization forming angles with the InSe *c* axis comprised between 65° and 85°.

III. RESULTS AND DISCUSSION

This section presents and discusses the results obtained by XAS and photoemission on the InSe/Pt interface. On the one side, discussion is focused on the analysis of the possible Pt diffusion into the InSe substrate, as obtained from XPS and XAS results. On the other side, we discuss the electronic nature and formation process of the barrier at the InSe/Pt interface, as Pt coverage increases, as obtained by ARPES measurements.

A. Platinum diffusion process

Figure 1 shows the In 3*d* spectra measured by XPS in InSe/Pt interfaces formed by successive Pt evaporations. In this series of spectra, it can be observed that progressive Pt deposition tends to downshift the In 3*d* core level (labeled *C*1) from that obtained for the clean InSe substrate. In addition, already at submonolayer Pt coverages, a new In 3*d* component (labeled *C*2) appears to develop at lower binding energies. Both In 3*d* components seem to downshift as the Pt coverage increases (see inset in Fig. 1) up to 1 ML of Pt is deposited. Nevertheless, beyond this Pt coverage, the *C*1 component tends to shift back by 0.2 eV whereas the *C*2 component downshifts until a constant shift of 1.4 eV is reached. Although these results reflect an intricate core level shift behavior with Pt deposition, they clearly indicate that Pt

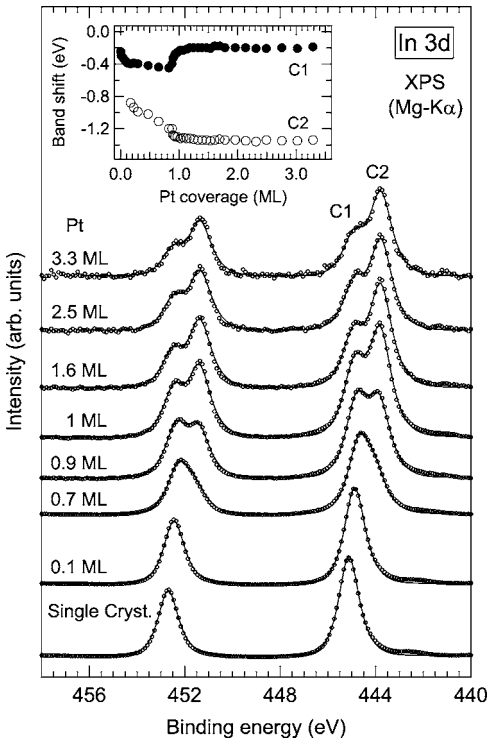

FIG. 1. In 3*d* spectra measured by XPS in InSe/Pt interfaces formed by Pt deposition. The nominal Pt coverage is indicated on each curve. Two core levels have been identified and labeled as *C*1 and *C*2. Solid lines are Gaussian fits to the experimental spectra, taking into account two core-level components. The inset shows the Pt-coverage dependence of the shift of both core levels with respect to that of the InSe substrate, as obtained by this fitting procedure.

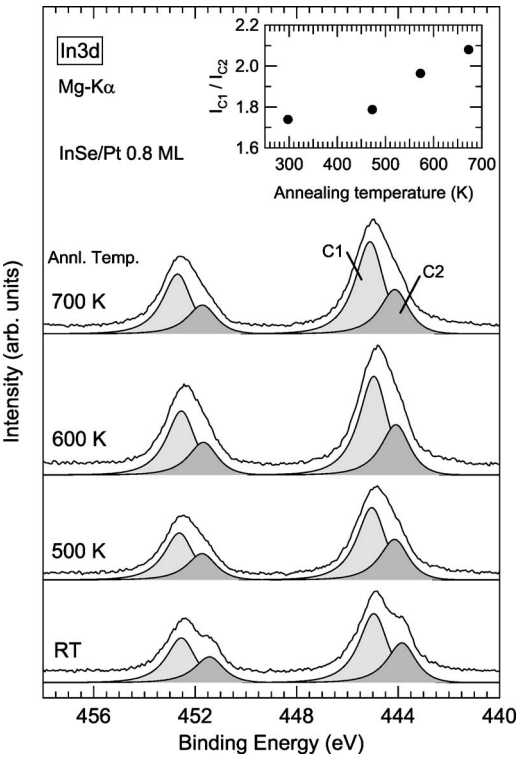

FIG. 2. In 3*d* spectra measured by XPS in InSe/Pt interfaces of 0.8-ML-thick Pt, after thermal treatment at temperatures indicated on each curve. The two core levels identified are those labeled as *C*1 and *C*2 in Fig. 1. Below each curve, it is shown the result of the Gaussian deconvolution of the spectra. The inset shows the annealing-temperature dependence of the relative intensity of the *C*1 and *C*2 components, as obtained by this deconvolution procedure.

reacts with the InSe surface even at early Pt coverage stages.

In order to clarify the origin of processes taking place at the InSe/Pt interface as Pt is deposited, XPS measurements on thermally treated samples have been carried out. It would be expected that the reaction mechanism was thermally activated in the case of a interdiffusion process. However, if Pt adatoms were bounded to the top InSe layer, chemical environment of the interface would not be expected to change gradually after thermal treatment. Figure 2 shows the In 3*d* spectra measured by XPS in InSe/Pt interfaces formed by a Pt deposition of 0.8 ML and annealed at different temperatures. In these spectra, traces from both *C*1 and *C*2 components can be observed in all treated samples. Nevertheless, the relative *C*1/*C*2 intensity, as obtained by Gaussian deconvolution of the spectra, appears to increase with the annealing temperature (see inset in Fig. 2). Moreover, it can be found that both In 3*d* core levels shift by 0.6 eV to higher binding energies as annealing temperature increases, which contrasts with the behavior observed with the increase of Pt coverage (Fig. 1). As the presence of this *C*2 component appears to be connected with the reaction process at the InSe/Pt interface, these results indicate that Pt is diffused into the InSe substrate, even at room temperature.

Once it has been established that Pt incorporates into the InSe substrate by diffusion, the atomic structure of the reacted InSe/Pt interface can be analyzed by XAS measurements. The Pt fluorescence signal of the samples studied here was detected even at the lowest coverage rates (around 0.4 ML), for which the Pt atom areal concentration on the InSe surface is of the order of 3×10^{14} cm^{-2}, just above the detection limit of ID26. The Pt LIII edge step was only 3% of the total signal and the extended x-ray absorption fine structure (EXAFS) oscillations could not be extracted from the background noise. The edge step increased proportionally to the coverage, reinforcing the deposition estimations based on photoemission (see Sec. II). In annealed samples, for Pt coverage rates larger than 0.4 ML, x-ray absorption near-edge structure (XANES) and EXAFS spectra can be extracted with a signal to noise ratio improving with the coverage rate. For the highest studied coverage (about 4 ML), the Pt edge step was about 50% of the background signal, and high quality XANES and EXAFS spectra could be measured, with an energy range up to 500 eV above the Pt LIII absorption edge.

We present in Fig. 3, upper panel, the EXAFS oscillations corresponding to a set of 4 ML samples annealed at different temperatures. The Fourier transformation of the EXAFS signal is presented in the lower panel of the same figure. The Fourier transformations have been carried out in a **k** domain between approximately 3 and 12.0 Å^{-1}, with a Bessel-type (τ=4) apodization window. The contribution of the first neighbor shell to the pair pseudodistribution function (PPDF) corresponds to the doublet structure observed between ap-

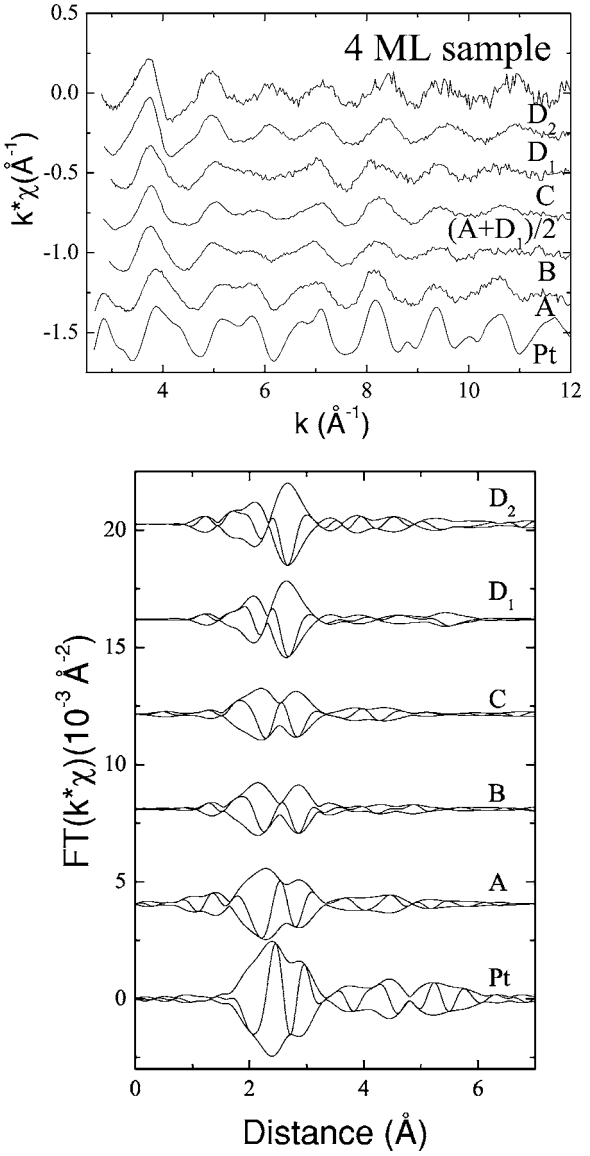

FIG. 3. Upper panel: EXAFS oscillations at the Pt-LIII edge. The spectra correspond to the sample with 4 ML coverage. Different thermal treatments or incidence angles ϕ have been used (A: No treatment, ϕ=67°; B: 500 K, ϕ=67°; C: 600 K, ϕ=65°; D_1: 700 K, ϕ=70°; D_2: 700 K, ϕ=37°). For comparison, we include also the spectrum of metallic Pt and the average spectrum calculated from A and D_1 curves [(A+D_1)/2]. Lower panel: Fourier transformation of the EXAFS signal. In both panels, the curves have been progressively shifted for clarity.

proximately 1.5 and 3.2 Å. The spectrum measured for the nonannealed sample (A curve) resembles that obtained for metallic Pt. The EXAFS analysis reveals no change in the Pt-Pt bonding distance with respect to metallic Pt, but static disorder has appeared to increase (see Table I for details). From these results it can be concluded that, at high Pt coverage, a disordered metallic Pt layer is formed on InSe.

This situation is drastically modified after thermal treatment (B–D_1 curves). The effect of annealing on the 4 ML sample is clearly appreciated in both EXAFS and PPDF features. The spectrum of the sample annealed at 700 K (D_1 curve) is completely different from the initial one (A curve), whereas samples annealed at lower temperatures (B and C curves) exhibit an intermediate situation between the extreme ones. The PPDF leads to the same conclusions. The doublet in the PPDF corresponding to the Pt first neighbor shell changes from samples A–D_1. In particular, the intensities of the peaks forming the doublet are interchanged in spectra D_1 with respect to those of spectrum A. XAS results, then, clearly point out a thermally enhanced Pt diffusion, coherently with that observed by XPS measurements (Fig. 2). On the other side, this diffusion process appears to be independent on the initial amount of Pt deposited. Figure 4 shows the XAS spectra measured in samples with a different Pt coverage, from 0.4 to 4 ML, after a 700 K thermal treatment. Since different samples exhibit similar spectra to that measured in the 4 ML sample, it is reasonable to think that at 700 K most of the Pt deposited has diffused into the InSe substrate. Therefore, Pt diffusion stage is irrespective of the quantity of Pt deposited, as would correspond to a thermally activated diffusion process.

The Pt diffusion process implies a change in the Pt neighborhood. We neglect the hypothesis of substitutional Pt on the basis of electronegativity and chemical bonding considerations. The Pt atoms should then occupy interstitial sites in the lattice. A description of the InSe structure can be found in the literature.[27–29] A detailed analysis of the InSe structure reveals that there are four interstitial positions, which are schematized in Fig. 5(a). In the interlayer space between the Se planes there are two sites, one octahedral (O) and one tetrahedral (T), where Pt would be sixfold and fourfold coordinated with Se, respectively. The Pt-Se distances would be $d^O_{\text{Pt-Se}}$=2.76 Å and $d^T_{\text{Pt-Se}}$=2.40 Å. In the intralayer space there are two prismatic (P) sites. The basis of the prism is an equilateral triangle defined by three In atoms. In both prismatic configurations Pt would be at the prism center, sixfold coordinated with In atoms at $d^P_{\text{Pt-In}}$=2.70 Å. In one of the configurations, the P_1, the nearest Se atoms to Pt are at $d^{P_1}_{\text{Pt-Se}}$=3.50 Å, whereas in the P_2 site they would be situated at $d^{P_2}_{\text{Pt-Se}}$=2.64 Å.

In order to distinguish between the four candidates for the Pt site, we have performed XANES simulations and EXAFS analysis. XANES simulations have been carried out using the real-space multiple scattering code implemented in the FEFF8 package.[30] We employed a self-consistent potential calculated using ~30 atoms clusters (6.0 Å around the absorbing atom) and the Hedin-Lundqvist energy-dependent self-energy. Full multiple scattering XANES calculations were performed using 87-atom clusters (~8.5 Å). The only nonstandard input to FEFF8 was the NOHOLE card, indicating that the calculations are carried out using ground state potentials, without a core hole. This option is often used on one electron LII, III calculations in order to reproduce the white line intensity.[31,32] Figure 5(b) shows the results of these calculations. We clearly appreciate that the spectra corresponding to the O and T configurations (those sites in the interlayer space) do not match the experimental spectra obtained in 700 K annealed samples, whereas simulations performed for the P_1 and P_2 intralayer sites are very similar to each other and both are compatible with the experimental spectra, al-

TABLE I. Structural parameters resulting from the EXAFS fit to the 4 ML spectra. We employ two different environments for the Pt atom, the one corresponding to the P_1 prismatic site and that of metallic Pt. x is the fraction of Pt atoms in the prismatic configuration. The sample labels are the same as in Fig. 3. The amplitude correction factor is $S_0^2=0.9$ in every fit. We have fixed those parameters whose error is not given in the table.

Sample	x	Coordination	Distance (Å)	Pseudo-DW (Å^2)	Energy shift (eV)
Metallic foil	0	$N_{Pt}=12$	2.77±0.01	0.0044±0.0010	6±2
A	0	$N_{Pt}=12$	2.77±0.01	0.0087±0.0011	6
B	0.5±0.2	$N_{In}=6$	2.76±0.03	0.0071	3
		$N_{Pt}=12$	2.81±0.02	0.0064±0.0020	6
C	0.5±0.2	$N_{In}=6$	2.75±0.03	0.0071	3
		$N_{Pt}=12$	2.80±0.02	0.0050±0.0020	6
D_1	1	$N_{In}=6$	2.77±0.02	0.0071±0.0011	3±2
D_2	1	$N_{In}=6$	2.76±0.02	0.0074±0.0018	3

though they do not fully reproduce it. The similarity observed between the P_1- and P_2-related simulations can be understood by the fact that, in both sites, Pt would be both surrounded by six heavy In atoms. In the P_2 site, the Se contribution to the spectrum is of minor importance, first of all because there are only two Se atoms, and secondly due to the lower atomic number of Se with respect to In.

The EXAFS oscillations provide complementary information. In Fig. 6 we show the differences between the PPDF involving In (P_1 and P_2 sites) or Se atoms (O or T sites, see inset). No matter the details of the site environment, the peak in the PPDF associated to first neighbors is always a doublet if the first shell is formed by In atoms and a singlet if it is constituted by Se atoms. As the experimental PPDF of the 700 K annealed samples (Figs. 3 and 6) evidences a doublet, we get additional support for the P_1 and P_2 described models. Turning to the quantitative analysis, in the EXAFS fit we employed phases and amplitudes obtained from a self consistent calculation with FEFF8. Table I summarizes the structural parameters obtained by this fitting procedure. The best fit to the 4 ML sample annealed at 700 K (D_1 curve in Fig. 3) involves 6 Pt atoms at $d_{Pt\text{-}In}=2.77\pm0.02$ Å (Fig. 6). The obtained distance is slightly longer than that predicted for the P_1 and P_2 sites in the unaltered lattice (2.70 Å). This means that the Pt diffusion into the InSe lattice in a prismatic site is accompanied by a small distortion of its environment, which, in any case, it appears not to be intense enough to segregate In atoms to the surface. The slight differences between the experimental and the calculated XANES spectra may be the

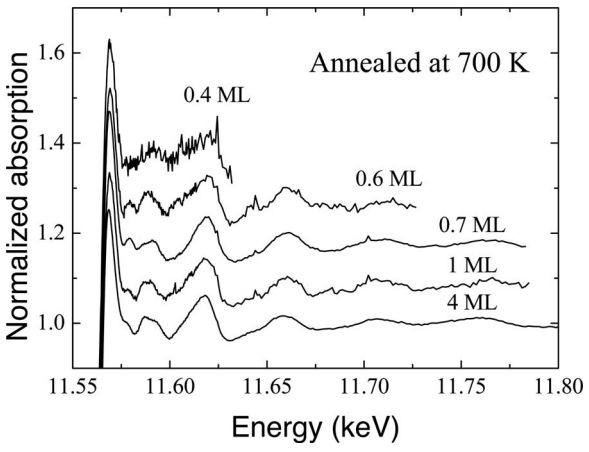

FIG. 4. XAS spectra of 700 K annealed samples with different initial Pt coverages. XAS spectra have been progressively shifted for clarity. The final state, where Pt has diffused, is the same no matter the initial coverage.

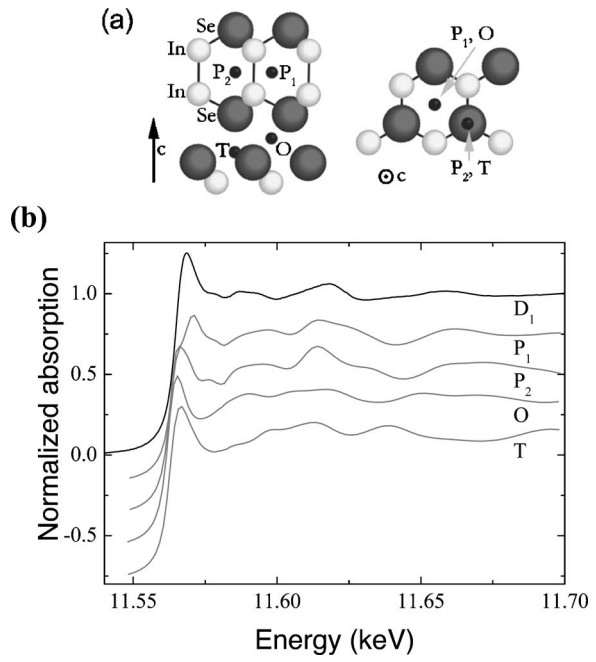

FIG. 5. (a) Possible configurations of Pt in the four existent interstitial sites of InSe. On the left, we show a [010] projection, perpendicular to the c axis of the InSe unit cell, and, on the right, a [001] projection. O and T correspond to sites where Pt is octahedrally or tetrahedrally coordinated with Se. In P_1 and P_2 configurations, Pt would be sixfold coordinated with In (see text for details). (b) XANES simulations calculated with the Pt atoms situated at these interstitial sites. We also show the experimental spectra (D_1) of the 4 ML sample annealed at 700 K, for comparison. The XANES simulations have been progressively downshifted for clarity.

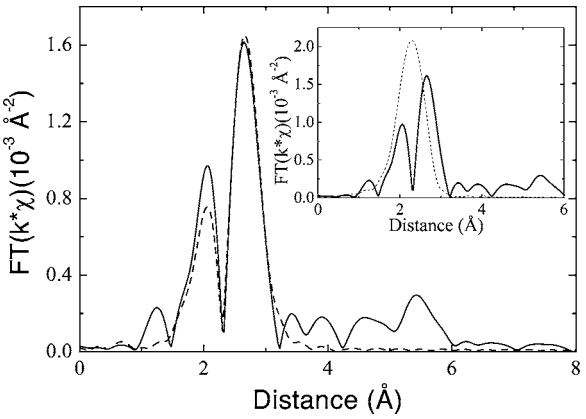

FIG. 6. Solid line: the experimental PPDF of the 700 K annealed 4 ML sample (the D_1-labeled curve in the lower panel of Fig. 3). Dashed line: the model where Pt is surrounded by six In atoms (P_1 and P_2 sites) explains the existence of a doublet in this experimental PPDF. The fit yields $N_{\mathrm{In}}=6$, $d_{\mathrm{Pt\text{-}In}}=2.77\pm0.02$ Å, $\sigma^2=0.0071\pm0.0011$ Å^2, and $E_0=3\pm2$ eV. Inset: Irrespective of the details, a model (O or T configurations) where Se surrounds Pt always implies a singlet in the PPDF, in contrast to the doublet observed in the experimental PPDF (solid line). The dashed line corresponds to a simulation with $N_{\mathrm{Se}}=6$, $d_{\mathrm{Pt\text{-}Se}}=2.64$ Å, $\sigma^2=0.0071$ Å^2, and $E_0=3$ eV.

result of the noninclusion of these distortions in our model. Additionally, in order to distinguish between the P_1 and P_2 sites, we have tried to include Se atoms in the EXAFS fit. The Pt-In bonding distance remained unaltered, but the structural parameters related to the Pt-Se contribution did not show a stable behavior. As in XANES simulations, the Pt-Se backscattered signal is too weak to extract reliable information. Therefore, at this point, we cannot distinguish if Pt occupies P_1 or P_2 sites, or both of them.

As we will see in Sec. III C, the acceptor character of isolated Pt atoms will be well established. Assuming this here, this would imply that Pt is as a Pt^- ion, probably with a $5d^{10}6s^1$ configuration. Based on electrostatic interaction considerations, it seems reasonable to assume that the most stable interstitial sites should be those in which the Pt^- ion is surrounded by a larger number of cations, i.e., the P_1 or P_2 sites [Fig. 5(a)]. Short-range repulsion between the electron clouds of In-In covalent bonds and Pt^- ions would give account of the slight increase of the Pt-In distances with respect to its value in an unoccupied site.

In the above discussion, analysis has been focused mainly on the spectra obtained in 700-K-annealed samples. In order to give a more precise perspective of the thermally activated behavior of the Pt diffusion process, we include in Table I the parameters obtained from the EXAFS fit of spectra corresponding to samples annealed at intermediate temperatures (B and C spectra of Fig. 3). We employed a two shell model where one of the shells represents Pt in a prismatic P_1 site, whereas the other is associated to nondiffused Pt remaining in a metallic configuration. To avoid, as much as possible, multiparameter correlation, several magnitudes have been fixed. The energy shifts have been set equal to those of metallic Pt and the D_1 spectrum (where we have seen that all Pt has diffused). Effective coordination numbers in the fit have been written in terms of the fraction of Pt which has diffused into the InSe matrix (x in Table I). Finally, the pseudo Debye-Waller corresponding to prismatic Pt has been fixed to 0.0071 Å. We obtain that half of the Pt atoms diffuse into the InSe matrix after thermal treatments of 500 and 600 K. In order to put into evidence this result, we have included in Fig. 3 the $(A+D_1)/2$ spectrum calculated by simple average of the extreme situations, which resembles the EXAFS oscillations obtained in B and C samples. On the other side, the remaining metallic Pt (nondiffused at intermediate annealing temperatures) seems to become slightly altered by the annealing treatment, as disorder decreases and the Pt-Pt distance increases (see Table I). However, the magnitude of the effect, as well as the experimental error, does not allow one to extract more solid conclusions. With respect to the prismatic Pt environment of the diffused Pt, there are no evidences of an intermediate behavior during the diffusion process.

Finally, we have also checked that XAS spectra in annealed samples do not depend on x-ray polarization. D_1 and D_2 spectra in Fig. 3 have been acquired with 70° and 37° incidence, respectively. We appreciate the similarities between both spectra. The EXAFS analysis, see Table I, revealed the same bonding distances and pseudo Debye-Waller factor. XANES simulations (not shown) did not evidence significant differences for this change in polarization. This behavior contrasts with the anisotropy found in the InSe XAS spectra at the Se or In K edges,[33] but, given the *effective* symmetric character of the four interstitial sites proposed, such polarization analysis does not help to distinguish between them.

B. Core-level and valence-band photoemission

The observed incorporation of the deposited Pt atoms into the InSe matrix at the interface drastically modifies the ideal scheme expected for an abrupt InSe/Pt Schottky barrier. In order to elucidate the mechanisms defining the origin of the InSe/Pt barrier, ARPES measurements performed at lower $h\nu$ than those carried out by XPS measurements (Fig. 1) is required, since the larger mean free path of photoelectrons excited by XPS may prevent for a precise determination of the barrier height at the interface. In fact, for such a little compact material, in comparison with the fcc ones, it would be expected an inelastic mean free path of photoelectrons of about 9, 15, and 70 Å for $h\nu=20$, 100, and 1250 eV,[34] respectively, that are even three times higher than that expected from the well-known universal curve.

Taking into account the present discussion, we show in Fig. 7 the In 4d and Se 3d core-level spectra measured by photoemission with $h\nu=100$ eV in InSe/Pt interfaces with different nominal Pt coverages. At first sight, it can be observed that both InSe core levels exhibit a similar behavior as Pt-coverage increases. Deposition of very small Pt amounts already leads to a pronounced shift of the spin-orbit doublets of 0.36 eV to lower binding energies with respect to those measured in the clean surface, signaling to a p-type band bending. In contrast to this abrupt behavior, successive Pt evaporations slightly shift the core levels to lower binding

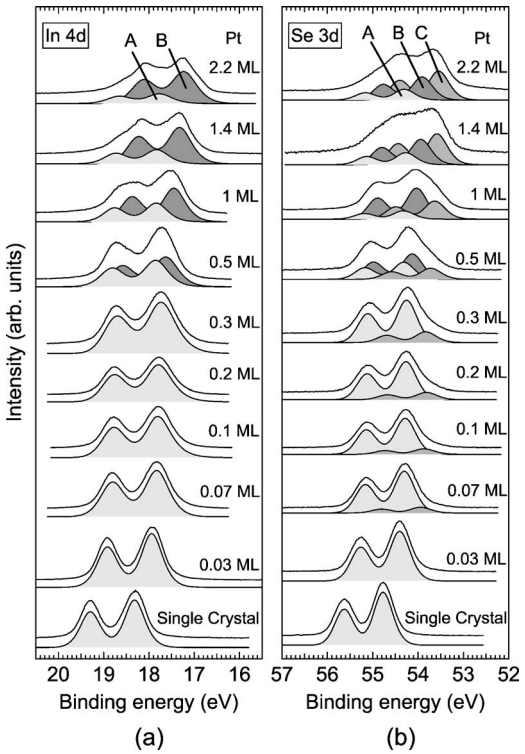

FIG. 7. EDCs of the core levels (a) In 4*d* and (b) Se 3*d* measured with $h\nu$=100 eV in InSe/Pt interfaces formed by successive evaporations of Pt on a InSe sample. The nominal Pt coverage is indicated on each curve. Different core-level components (labeled as *A*, *B*, and *C*) have been identified. Under each spectrum it is shown the result of its Voigt decomposition into the different components observed.

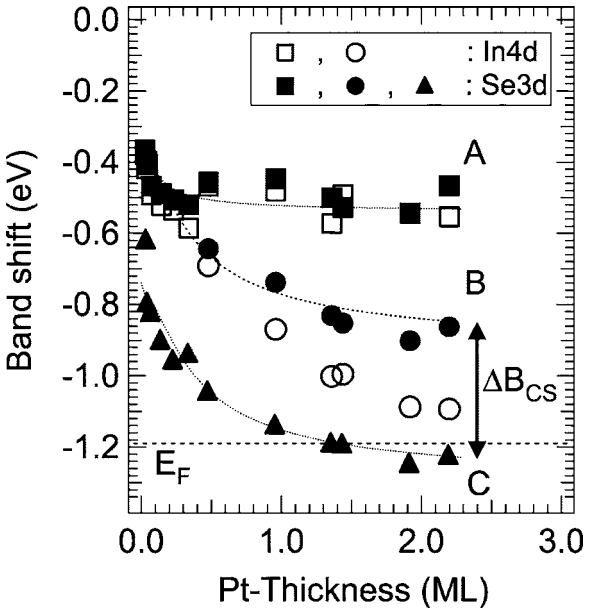

FIG. 8. InSe-band shift as a function of the Pt coverage, as extracted from the Pt-coverage dependence of the position of the two components resolved in the core level spectra shown in Fig. 7. Dotted lines are guides for the eyes. Note that the dashed line corresponding to the experimental trend exhibited by *C* is that of *B* downshifted by ΔB_{CS}=0.38 eV. Dashed line indicates the position of the E_F in the InSe samples used here.

energies. As it was observed by XPS (Fig. 1), beyond a certain Pt coverage an additional feature can be observed to develop at lower binding energies, for both InSe core levels, causing that the spectra progressively shift to lower binding energies as Pt coverage increases.

These results clearly evidence, again, that Pt reacts with the InSe surface. In any case, this process appears not to strongly disturb the InSe layer structure at the interface, coherently to that obtained by XAS measurements, since no trace from metallic indium has been detected by photoemission as would be expected in an indium segregation process.

In order to further discuss the role of Pt in the formation of the InSe/Pt interface, a Voigt-fitting procedure has been adopted to decompose each In 4*d* and Se 3*d* spectrum of Fig. 7 into several spin-orbit doublets. For this fitting procedure, it has been assumed that each doublet is defined by two peaks of the same width, with a intensity ratio given by the relative $(2J+1)$ degeneracy of the states, and with the same spin-orbit splitting as that obtained from the clean surface (0.97 and 0.86 eV for the In 4*d* and Se 3*d*, respectively). From this fitting procedure, it has been obtained that the experimental In 4*d* spectra are quite well reproduced by taking into account up to two core-level components, whereas three core-level components have to be considered, for Pt coverages higher than 0.5 ML, in order to reproduce the Se 3*d* series of spectra. These core level components appear to be slightly widened with respect to those of the clean surface, due to band bending effects, which exhibit a different binding energy evolution as Pt coverage increases. At low Pt coverages, only one component can be resolved (the *A* feature) for both InSe core levels. Nevertheless, already at a Pt coverage of ~0.07 ML, a weak component (*C* feature) can be observed to develop besides the most prominent one in the Se 3*d* spectra, at lower binding energies, which appears to be enhanced as the Pt coverage increases. At a Pt coverage of ~0.5 ML, the main component of both series of spectra (the *A* one) seems to split into two components (*A* and *B*). One of them, the *A* one, appears to tend to vanish in favor of the *B* one, which shifts to lower binding energies as Pt coverage increases whereas the *A* one no longer downshifts.

Figure 8 shows the Pt-coverage dependence of the shift of these components with respect to those measured in the clean InSe substrate, as obtained from fitting of both In 4*d* and Se 3*d* spectra. These results reveal some facts that should be remarked, besides the abrupt *p*-type shift of the InSe core levels observed at the lowest Pt deposition. On the one side, it can be observed that both *A* components progressively downshift by 0.6 eV, which would correspond to an InSe valence band position at the interface close to the middle of the InSe band gap (E_g=1.3 eV).[35] On the other hand, it appears that the behavior of the *C* component would correspond to that of a degenerate interface, since the E_F is 110 meV far from the conduction band minimum in these *n*-InSe samples. Nevertheless, it should be noticed that the Pt-coverage dependence of the shift of the *B* and *C* components of the Se 3*d* are similar, but shifted by 0.38 eV. With regards to the shift of the *B* component of the In 4*d*, its

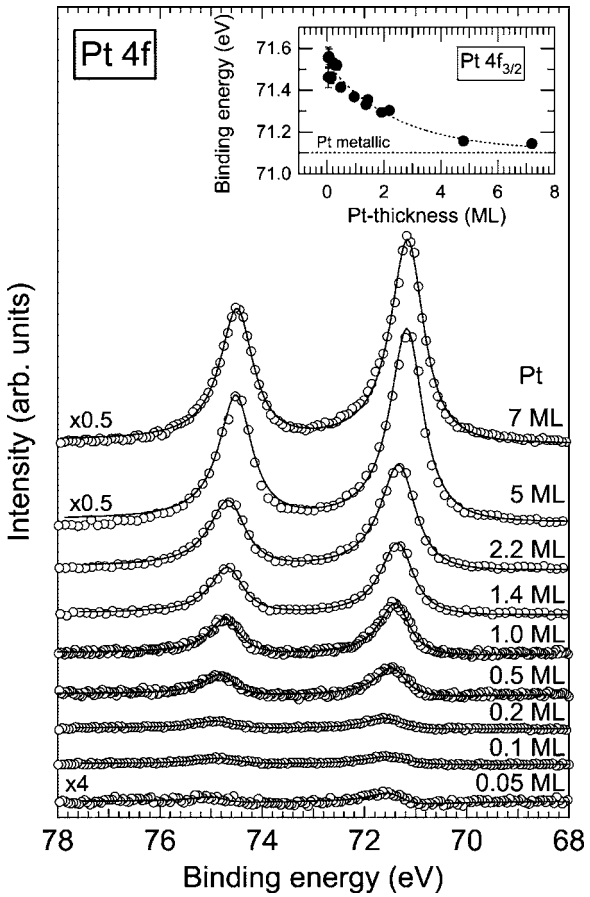

FIG. 9. EDCs of the Pt 4*f* core level measured with $h\nu = 150$ eV in InSe/Pt interfaces with different amounts of Pt deposited. All spectra have been normalized to a constant background. The nominal Pt coverage is indicated on each curve. Solid lines are Doniach-Šunjić fitting curves. The inset shows the Pt-coverage dependence of the binding energy of this core level, as extracted from this fitting process. The dotted line is a guide for the eyes.

Pt-coverage dependence appears to reflect an intermediate behavior between those observed for the *B* and *C* components of the Se 3*d*.

The evolution observed for the InSe core levels as Pt is deposited contrasts with that obtained for these of Pt. Figure 9 shows the Pt 4*f* spectra obtained by photoemission in InSe/Pt interfaces formed by successive evaporations of Pt on an InSe sample. In these spectra, it can be observed that a clear Pt 4*f* spin orbit doublet develops and shifts to lower binding energies as Pt is deposited, which exhibits a clearly asymmetric line shape for the highest Pt coverages. This asymmetric profile may be attributable to a superposition of different lines. Nevertheless, this fact can be readily explained by collective screening of the conduction electrons, as is well known for simple metals,[36] since bulk Pt layers are expected to be formed at these high Pt coverages. Therefore, it appears that, in contrast to that obtained for the InSe core levels shown in Fig. 7, only one Pt 4*f* component seems to develop in these spectra as Pt is deposited. Since we are interested in the energy shift caused by Pt deposition of this core level, we have fitted the experimental spectra to a Pt 4*f* spin-orbit doublet with a line shape defined by the so-called Doniach-Šunjić line shape, for all Pt coverages, taking into account that the Pt 4*f* spin-orbit splitting is that obtained for a bulk Pt overlayer (3.33 eV). The results of this fitting procedure are displayed in Fig. 9, which reproduce the experimental spectra. The Pt-coverage dependence of the Pt 4*f* binding energy is shown in the inset of Fig. 9, as obtained from this fitting procedure. These results reflect that this core level progressively shifts to lower binding energies as Pt is deposited, tending to a value close to that expected for a bulklike metallic Pt layer for nominal Pt coverages higher than 4 ML.[37]

These photoemission results can be directly connected with the atomic structure of the InSe/Pt interface. The fact that only two components are observed in the In 4*d* deep levels, in contrast to that obtained for the Se 3*d* spectra (Fig. 7), can be understood on the basis of the configuration of the trigonal-prismatic intralayer sites and chemical shift effects. For both P_1 and P_2 sites, only one relative position is possible for In atoms with respect to Pt at a close interacting distance, whose first neighbor position is at 2.70 Å. In any other position, In atoms would be at distances longer than 5 Å from the Pt atoms. This is not the case of the Se atoms, for which there are two possibilities, i.e., those in which the nearest Se atoms to Pt are at 3.50 and 2.64 Å in the P_1 and P_2 configurations, respectively. Therefore, it appears that, among all core-level components observed (Fig. 7), the *B* and *C* components of the Se 3*d*, on the one side, and the *B* component of the In 4*d*, on the other side, are related to the incorporation of Pt into the two different prismatic sites, since the former behave similar to each other as the Pt coverage increases but shifted by $\Delta B_{CS} = 0.38$ eV and the latter exhibits an intermediate behavior between them (Fig. 8).

These two Se 3*d* components can be univocally related with each one of the prismatic sites by taking into account chemical shift arguments. Since it would be expected that the Se 3*d* chemical shift induced by the Pt atoms should be the higher the shorter the Pt-Se distance is, the appearance of the *B* and *C* components of the Se 3*d* can be tentatively connected with the incorporation of Pt atoms in the P_1 and P_2 sites, respectively. Accordingly with this assignment, it appears that Pt atoms tend to occupy one of the prismatic sites rather than the other as they incorporate into InSe, as can be concluded from the evolution of the Se 3*d* core levels as Pt deposition increases (Fig. 7). At very low Pt coverages, only traces from the *C* component of the Se 3*d* can be resolved, besides the main *A*-labeled component. As Pt coverage increases to 0.5 ML, the *B* component splits from the main component, revealing that its relative contribution to the Se 3*d* spectra was really more important than that of the *C* component at lower Pt coverages but masked by the *A* component. As Pt coverage exceeds 0.5 ML, the *C* component rapidly develops, contributing to the Se 3*d* spectra as much as the *B* one. These results evidence, first, that the longer distance from Se to Pt atoms in the P_1 configuration (a 30% longer than that in the P_2 one) makes chemical shift effects on the *B* component be negligible and, on the contrary, these are determinant on the appearance of the *C* component, since the *B* component is the only one of them that develops from the nonreacted component (the *A* one). Secondly, these results also point out that, at initial stages of Pt coverage, Pt

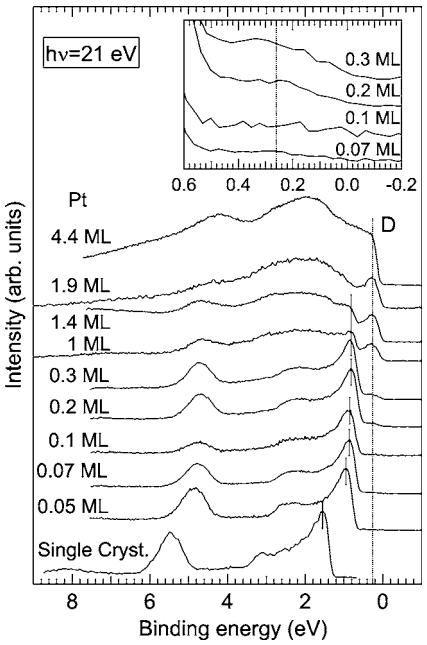

FIG. 10. Normal-emission valence-band EDCs measured with $h\nu$=21 eV in InSe/Pt interfaces formed with different amounts of Pt deposited. The nominal Pt coverage is indicated on each spectrum. The position of the highest InSe valence band is indicated by solid bars. Dotted line indicates the position of the band close to the E_F emerging with increasing Pt coverage, labeled as D. The inset shows, in an expanded scale, some of these spectra pointing out the detection onset of this band.

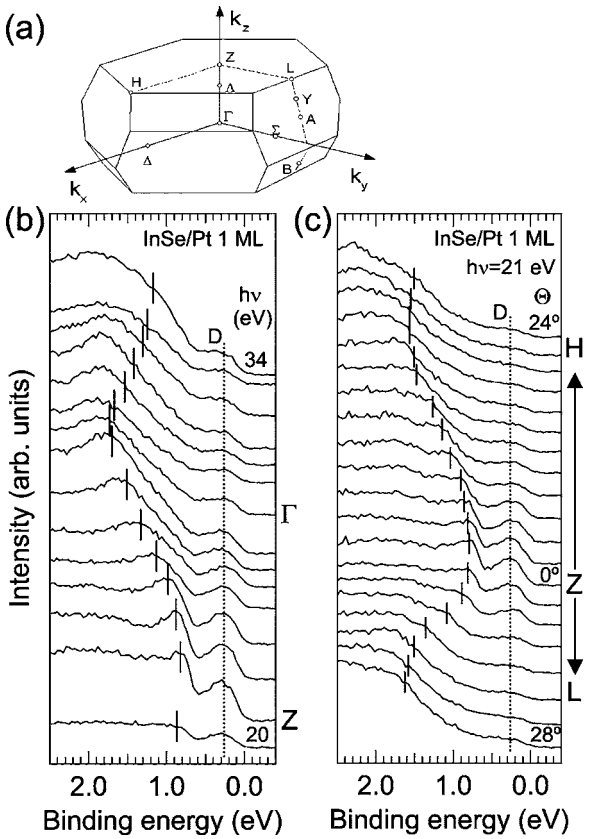

FIG. 11. (a) InSe rhombohedral Brillouin zone, in which the main points are indicated. (b) Normal-emission valence-band EDCs measured by ARPES with different excitation energies in a InSe/Pt interface with a Pt coverage of 1 ML. In this way, the $Z\Gamma$ direction is scanned by ARPES. (c) Valence-band EDCs measured by ARPES with $h\nu$=21 eV in the same InSe/Pt interface. For this selected $h\nu$, both ZH and ZL directions have been scanned by ARPES. Dispersion of the highest InSe valence band is indicated by solid bars. Position of the nondispersing band appearing close to the E_F is indicated by a dotted line.

atoms mostly occupy the prismatic P_1 site at low Pt coverages, whereas both P_1 and P_2 sites tend to be occupied in a similar proportion as Pt coverage increases.

Let us discuss now the fact that the Pt 4f peak exhibits only one core-level component (Fig. 9). From XAS results we unambiguously know that Pt atoms are in two different configurations, i.e., metallic Pt in surface clusters and interstitial Pt atoms in P_1 or P_2 prismatic intralayer sites. As photoemission results are also unambiguous in their showing a single component of the Pt 4f peak, the physical conclusion deriving from both results is that Pt atoms have the same chemical shift in both configurations (or the difference between the respective chemical shifts is too small to be detected with our experimental sensitivity). This conclusion is indeed coherent with the fact that, in both configurations, Pt atoms are mainly surrounded by cations at virtually the same distance. One can find in the literature examples of atoms exhibiting practically indistinguishable chemical shifts in very different site configurations (i.e., Ga atoms have the same chemical shift in tetrahedral or octahedral configuration with oxygen).[38] Consequently, Pt 4f appears to be the peak of choice in order to measure the purely electrostatic shift associated to the built in potential of the depletion zone.

Photoemission measurements of the valence band can shed some light on the nature of mechanisms determining the electronic behavior of these interfaces. Figure 10 shows the valence band spectra measured with $h\nu$=21 eV in InSe/Pt interfaces formed by incremental Pt coverage. With the selected $h\nu$, it is expected ARPES to probe points of the InSe valence band close to the Z point of the InSe Brillouin zone [see Fig. 11(a)],[39] that is, at the point where the InSe valence band maximum (VBM) is found.[40,41] In fact, for the clean InSe spectrum, the top of the valence band lies at 1.21 eV from the E_F, as would be expected for these n-doped InSe samples. In this way, photoemission measurements carried out in these interfaces with this $h\nu$ directly monitor electronic states determining the semiconducting properties of the InSe surface and how they could be altered by the Pt deposition. Keeping this in mind, it can be observed that, after deposition of a very small amount of Pt, the whole InSe spectrum is already shifted towards the E_F by 0.50 eV, without any additional observable feature originated by the Pt deposition. Opposite to this initial abrupt trend, further Pt depositions appear to increase the shift of the InSe spectra only by 0.2 eV more. This behavior of the InSe valence band resembles that obtained for the B component of the Se 3d (Fig. 8), for the same Pt-coverage range, however, the observed InSe valence band shift seems to be slightly lower.

The effects of Pt deposition on the InSe valence band spectra are not only limited to valence band shifts. In addi-

tion to these results, it appears that a new band (labeled as D) progressively emerges at 0.26 eV from the E_F as Pt is deposited, which can be resolved even for submonolayer Pt coverages (see inset in Fig. 10). These states located at the InSe forbidden gap seem to be connected with the reaction processes taking place at the interface which are also responsible for the appearance of the C component of the Se $3d$ (Fig. 7), since both results point out a degenerate behavior of the InSe side of the interface (Fig. 8). In order to analyze the electronic nature of this degenerate band, valence-band spectra of these InSe/Pt interfaces have been measured by ARPES along different high-symmetry directions of the InSe Brillouin zone [Fig. 11(a)]. The results of these ARPES measurements are shown in Figs. 11(b) and 11(c), for an InSe/Pt interface with a Pt coverage of 1.0 ML. In these spectra, it can be observed that the highest InSe valence band disperses from its maximum at Z to its minimum at Γ along the $Z\Gamma$ high-symmetry direction,[40,41] as well as to higher binding energies along the ZH and ZL high-symmetry directions. In contrast to this dispersing behavior of the InSe valence band, the D band is nondispersing along any high-symmetry direction. These results indicate that Pt-InSe reaction processes at the interface give rise to the appearance of localized states within the InSe band gap, which would play a key role in the formation of the electronic barrier at the InSe/Pt interface.

The appearance of the D band can be explained in terms of the InSe valence band structure. First of all, it is worth noticing that, in spite of In atoms being in first-neighbor position, the In-Pt interaction cannot have a strong effect on the VBM, as the only band with predominant In s character is the one associated to the tight In-In covalent bond located at about 4 eV below the VBM. The states at the VBM have mainly nonbonding Se p_z character and are responsible for the interlayer interaction. Gomes da Costa *et al.*[40] have shown that the charge density corresponding to the upper valence band extends also inside the layers reaching the P_2 site. The presence of Pt atoms in these sites can perturb states at the VBM as the C_{3v} symmetry of γ-InSe allows mixing of Pt s and Se p_z states, both belonging to the fully symmetric $\Gamma_1(A_1)$ representation. It is well known that the upper InSe valence band has a large dispersion along the ΓZ high symmetry direction,[40,41] as a clear signal of extended states across the InSe layers. Then, the presence of a localized band (the D band) could be described as a *bonding* combination of these states in a Se-Pt-Se *molecule* formed by a Pt atom in a P_2 site and its two first Se neighbors.

The presence of this band close to the E_F connected with the incorporation of Pt atoms in a P_2 site would contribute to explain the different occupation probability of the prismatic sites, as revealed from the relative intensity evolution of the B and C components of the Se $3d$ (Fig. 7). A Pt atom in a P_2 site gives rise to states with an orbital behavior mainly derived from Se-related orbitals (Figs. 7 and 10), such as the D band from p_z states and the C band from $3d$ states. This fact indicates that InSe states involved in the Pt-InSe reaction states are raised in energy with respect to those of InSe. Therefore, it would be reasonable to expect that the extra energy cost of this process, supplied by the system, made Pt occupation of P_1 sites more probable than the P_2 ones, at low Pt coverage stages. Only when some fraction of these sites at the InSe top layers are already occupied and deeper Pt diffusion is not energetically favored, subsequent Pt atoms tend to occupy the P_2 site, enhancing the relative contribution of the C component to the Se $3d$ spectra (Fig. 7).

C. Electronic structure at the InSe/Pt interface: Role of platinum

At this point, it clearly appears that the electronic behavior, as well as the structure, of the InSe/Pt interface are far from those expected from a ideal InSe/Pt Schottky junction. In the Schottky limit, it would be expected a band bending close to the band gap for the n-InSe samples used here, assuming that the work function of polycrystalline Pt (no LEED pattern was observed for a bulk Pt layer) is of 5.5 eV and the InSe electron affinity is of the order of 4 eV.[16,42] Nevertheless, the above reported results indicate that Pt incorporates into the InSe layers, modifying this ideal band diagram of the InSe/Pt interface.

The question is now how to connect the incorporation of Pt in InSe prismatic intralayer positions with the formation of an electronic barrier at the InSe/Pt interface even before the onset of metallization expected for a bulklike Pt layer on the InSe substrate. In order to answer this question, we propose the scheme of the InSe/Pt-barrier formation illustrated in Fig. 12, in which three different regimes can be established depending on the Pt-coverage degree.

At very early stages of Pt deposition [Fig. 12(a)], an abrupt shift of the InSe bands of about 0.5 eV has been observed (Figs. 8 and 10), turning the InSe/Pt interface into intrinsic. A similar abrupt behavior at initial stages of metal deposition and a subsequent E_F pinning as metal coverage increases have been already observed in III-V semiconductors.[43] These results were explained by defects introduced by the adsorbates independently of reactivity of the interface.[43] Nevertheless, in nonreacted interfaces with a low defect density, E_F pinning processes appeared to be dominated by metal-induced gap states.[44] In the case of the InSe/Pt system, none of these mechanisms appear to be determinant in the barrier formation at the InSe/Pt interface since (i) photoemission is a rather defect-sensitive technique and the shape of all components of the InSe core levels, as well as the InSe valence band, appear to remain practically unaltered after Pt deposition (Figs. 7 and 10) and (ii) the incorporation of Pt to the InSe matrix discards the possibility to identify the band appearing within the InSe band gap to metal-induced gap states in its proper sense, that is, to states induced by the proximity to a metal.[2,3]

From our results, it appears that Pt atoms incorporate into the InSe matrix at the very early stages of Pt coverage even at room temperature. In this case, it would be expected that most of the Pt atoms were isolated from each other into the InSe matrix. Under these conditions and coherently to that expected by electronegativity arguments, these Pt atoms would act as surface p-dopant agents, giving rise to a p-InSe region at the interface. Acceptor states are then created within the InSe band gap. These localized states trap free electrons (so creating a space charge that gives rise to the band bending potential) and only the overall electrostatic

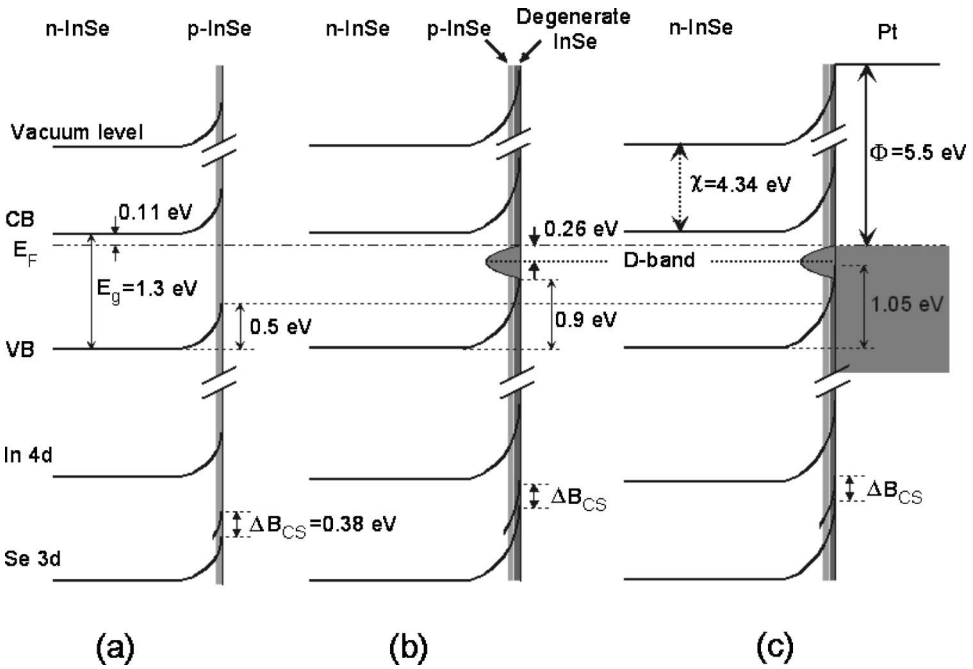

FIG. 12. Schematic model of the InSe/Pt barrier formation at the interface, as Pt content increases from (a) to (c).

shift due to the built-in potential of the related depletion zone is observed, as reflects the presence of a unique component (the *A* one) in the Se 3*d* and In 4*d* spectra at these very low Pt coverage stages (Fig. 7).

The role of Pt as a dopant agent in InSe can be analyzed by solving the Poisson's equation taking into account the surface concentration of acceptor centers N_{Pt} introduced by the Pt atoms. These acceptors trap electrons giving rise to a space charge zone of width W and barrier height E_B connected by the relation[45]

$$E_B = \frac{e^2 W^2 N_d}{2\epsilon}, \tag{1}$$

where e is the electron charge and ϵ is the InSe permittivity. This relation can be expressed as a function of N_{Pt} by

$$E_B = \frac{e^2 {N_{\mathrm{Pt}}}^2}{2\epsilon N_d}. \tag{2}$$

For the *n*-InSe samples used here,[46] it results from Eq. (2) that the diffusion of only 4.6×10^{-4} ML of Pt into the InSe matrix would be enough to produce a band bending of 1.1 eV, that is, to make the interface degenerate. In this context, it is not surprising that a small fraction of the deposited Pt atoms which diffuses into the InSe substrate would give rise to an abrupt band shift at initial stages of Pt deposition, by a *p*-doping mechanism. Nevertheless, this simple mechanism does not account by itself for the further evolution of the InSe bands as Pt is deposited.

In the present *p*-doping model, it may be objected that as the valence band runs closer to the E_F the hole concentration at the interface is no longer negligible and, consequently, it would be required a larger Pt amount incorporated into the InSe matrix to progressively increase E_B. This fact would produce a saturationlike effect of the band bending shift with increasing Pt that could explain the experimental results (Figs. 8 and 10). In order to determine the role of this hole accumulation layer, Poisson's equation should be solved incorporating the hole contribution to obtain the N_{Pt} dependence of E_B. Nevertheless, an approximate expression of the surface hole density can be obtained and Eq. (2) can be rewritten as

$$N_{\mathrm{Pt}} \simeq \frac{\sqrt{2\epsilon N_d E_B}}{e} + \delta \frac{N_c N_v}{N_d} e^{-(E_g - E_B)/k_B T}, \tag{3}$$

where δ is the hole confinement length in the two-dimensional system and $N_{c,v}$ stand for the effective density of states of the conduction and valence band, respectively. Taking into account that escape length of photoelectrons is a few tens of Å for the $h\nu$ selected in our photoemission measurements and that several core level components have been resolved in the spectra shown in Fig. 7, the *A*-labeled component coming from an intrinsic local environment, it can be assumed that δ is of the order of the photoelectron escape length. Under these assumptions and considering carrier-effective-mass values reported in the literature,[47] the E_B behavior appears to be basically determined by the second term in Eq. (3) for E_B values higher than 1.1 eV, which exceeds that observed for the InSe bands (Figs. 8 and 10). Therefore, it appears that the origin of the smooth band shift observed as Pt coverage increases stems from a mechanism connected with the Pt incorporation to the InSe matrix different from a doping one.

At this point, it appears that the barrier evolution at the interface for intermediate Pt coverages (from 0.03 to 2 ML) is mostly controlled by Pt-InSe reaction processes [Fig. 12(b)]. As Pt coverage increases, the concentration of Pt atoms in prismatic intralayer positions increases and chemically shifted components corresponding to In or Se atoms in first neighbor position with respect to Pt are clearly observed (Fig. 7). On the other side, the initial localized (acceptor)

state begins to develop, giving rise to the *D*-labeled band close to the E_F (Fig. 10) trapping now electrons from the InSe valence band. This band appears to control further barrier evolution, giving rise to a E_B=0.9 eV as obtained from the evolution of the *B* component of the Se 3*d* (Fig. 8). In this context, it can be understood the fact observed that the InSe valence band appeared to be nearly clamped as Pt deposition increases (Fig. 10), since the Se p_z states of the InSe valence band progressively turn into localized p_z states (the *D* band), masking the inherent InSe band bending behavior reflected by the InSe core levels (Fig. 8). On the other side, the formation of a degenerate layer would also explain the splitting of the *A*-labeled InSe core levels observed at a Pt coverage of 0.5 ML (Fig. 7): These appearing at higher binding energies (the *A* ones) would come from deep InSe layers (they attenuate as the degenerate layer grows) whereas those appearing at lower binding energies would correspond to the In and Se atoms in a Pt-InSe reacted environment.

If a degenerate (semimetallic) layer became completely formed, subsequent Pt deposition would not further alter the electronic barrier at the interface. Nevertheless, the Pt 4*f* core level appears to still downshift by 0.15 eV as the Pt coverage exceeds 2 ML. Moreover, comparing the behavior of both InSe and Pt core levels as the Pt coverage increases up to 2 ML (Fig. 8 and inset of Fig. 9) it can be found that the progressive shift of the Pt 4*f* follows that obtained for the *B* component of the Se 3*d*. These results indicate that, in spite of the fact that the barrier formation is mostly determined by reaction processes taking place at the InSe side of the InSe/Pt interface at low Pt coverages, the contribution from a emerging bulklike Pt layer cannot be completely discarded [Fig. 12(c)]. These results reflect that the formation of a bulklike Pt layer finally determines the InSe/Pt E_B, as would be expected for a Schottky barrier, giving rise to a final electronic barrier of E_B=1.05 eV, as extracted from the Pt 4*f* core level shift observed. These results allow us to determine the InSe electron affinity to be 4.34 eV, assuming that the Pt work function is of 5.5 eV.[42]

IV. CONCLUSIONS

The atomic structure and the electronic nature of the InSe/Pt interface have been studied by x-ray absorption spectroscopy and angle-resolved photoemission, respectively. By x-ray absorption spectroscopy, it has been found that Pt incorporates into the InSe matrix even at room temperature, without indium segregation to the surface, in the two trigonal-prismatic sites existing within the InSe layer. These intralayer positions are located at the center of the prism defined by the six indium atoms of the extreme sheets of the InSe hexagonal cell. These sites have been found to be nonequivalent energetically. This fact produces that, at initial stages of Pt diffusion, the occupation of the site with a lower interaction with the InSe orbitals is favored. Nevertheless, as the Pt coverage rate increases, the site with a stronger interaction with the Se orbitals is also occupied.

Structural processes taking place at the InSe/Pt interface have their counterpart in the InSe/Pt barrier formation as Pt is deposited, as revealed by photoemission measurements. At initial stages of Pt deposition, the incorporated Pt atoms act as isolated surface acceptors which turn the interface into intrinsic. Beyond a certain Pt coverage, the electronic barrier formation is now controlled by an emerging degenerate InSe region due to the formation of a band within the InSe band gap. The origin of this band has been attributed to the Pt-induced localization of extended states from the InSe valence band maximum, at the *Z* point of its Brillouin zone. The presence of this band has appeared to determine the InSe/Pt barrier height before the onset of metallization expected by the formation of a bulklike Pt layer onto the InSe substrate. Nevertheless, in order to completely understand the electronic barrier formation of the InSe/Pt interface, the contribution from a bulklike layer must be taken into account.

The atomic structure of the InSe/Pt interface has appeared to be quite far from that expected for an ideal InSe/Pt interface and the formation of a final bulklike Pt layer scarcely contributes to the electron barrier height at the interface. Nevertheless, the final InSe/Pt barrier height appears to be that expected for an abrupt InSe/Pt Schottky one.

Finally we would like to remark that, as the incorporation of Pt into the InSe substrate is thermally activated, this system opens new possibilities to explore a wide range of interfaces with completely different structural configurations, by controlling the deposition temperature, whose electronic behavior may be determined by other interface processes differing from those described in this work.

ACKNOWLEDGMENTS

This work was financed by the Large Scale Facilities program of the EU to LURE and ESRF. Part of this work was supported by the Ministerio de Ciencia y Tecnología of Spain (Project Nos. MAT2002-04539-C02-01 and MAT2002-03431).

*Electronic address: Juan.F.Sanchez@uv.es

[1] R. T. Tung, Phys. Rev. Lett. **84**, 6078 (2000).

[2] D. A. Muller, D. A. Shashkov, R. Benedek, L. H. Yang, J. Silcox, and D. N. Seidman, Phys. Rev. Lett. **80**, 4741 (1998).

[3] M. Kiguchi, R. Arita, G. Yoshikawa, Y. Tanida, M. Katayama, K. Saiki, A. Koma, and H. Aoki, Phys. Rev. Lett. **90**, 196803 (2003).

[4] S. Hasegawa, X. Tong, S. Takeda, N. Sato, and T. Nagao, Prog. Surf. Sci. **60**, 89 (1999).

[5] W. E. Spicer, I. Lindau, P. Skeath, and C. Y. Su, J. Vac. Sci. Technol. **17**, 1019 (1980).

[6] M. Yamada, A. K. Wahi, T. Kendelewicz, and W. E. Spicer, Phys. Rev. B **45**, 3600 (1992).

[7] C. Lamberti, E. Groppo, C. Prestipino, S. Casassa, A. M. Ferrari,

C. Pisani, C. Giovanardi, P. Luches, S. Valeri, and F. Boscherini, Phys. Rev. Lett. **91**, 046101 (2003).
[8] G. Barcaro, A. Fortunelli, F. Nita, and R. Ferrando, Phys. Rev. Lett. **95**, 246103 (2005).
[9] S. Schintke, S. Messerli, M. Pivetta, F. Patthey, L. Libioulle, M. Stengel, A. De Vita, and W.-D. Schneider, Phys. Rev. Lett. **87**, 276801 (2001).
[10] D. A. Ricci, T. Miller, and T.-C. Chiang, Phys. Rev. Lett. **93**, 136801 (2004).
[11] H. L. Meyerheim, R. Popescu, J. Kirschner, N. Jedrecy, M. Sauvage-Simkin, B. Heinrich, and R. Pinchaux, Phys. Rev. Lett. **87**, 076102 (2001).
[12] Y. T. Matulevich, T. J. Vink, and P. A. Zeijlmans van Emmichoven, Phys. Rev. Lett. **89**, 167601 (2002).
[13] A. Koma, Thin Solid Films **216**, 72 (1992).
[14] W. C. Eckhoff, R. S. Putnam, S. Wang, R. F. Curl, and F. K. Tittel, Appl. Phys. A: Mater. Sci. Process. **63**, 437 (1996).
[15] M. A. Hernández, J. F. Sánchez, M. V. Andrés, A. Segura, and V. Muñoz, Opt. Pura Apl. **26**, 152 (1993).
[16] A. Segura, J. P. Guesdon, J. M. Besson, and A. Chevy, J. Appl. Phys. **54**, 876 (1983); J. Martínez-Pastor, A. Segura, J. L. Valdés, and A. Chevy, *ibid.* **62**, 1477 (1987).
[17] J. F. Sánchez-Royo, A. Segura, O. Lang, E. Schaar, C. Pettenkofer, W. Jaegermann, L. Roa, and A. Chevy, J. Appl. Phys. **90**, 2818 (2001).
[18] V. K. Lukyanyuk, M. V. Tivarnitskii, and Z. D. Kovalyuk, Phys. Status Solidi A **104**, K41 (1987).
[19] M. Balkanski, C. Julien, and J. Y. Emery, J. Power Sources **26**, 615 (1989).
[20] T. Shimada, F. S. Ouchi, and A. Koma, Jpn. J. Appl. Phys., Part 1 **32**, 1182 (1993); S. Tiefenbacher, H. Sehnert, C. Pettenkofer, and W. Jaegermann, Surf. Sci. **318**, L1161 (1994).
[21] T. Löher, K. Ueno, and A. Koma, Appl. Surf. Sci. **130–132**, 334 (1998).
[22] B. Ulrich, A. Koma, T. Löher, and T. Kobayashi, Solid State Commun. **107**, 209 (1998).
[23] X. Zaoui, R. Mamy, and A. Chevy, Surf. Sci. **204**, 174 (1988).
[24] O. Lang, C. Pettenkofer, J. F. Sánchez-Royo, A. Segura, A. Klein, and W. Jaegermann, J. Appl. Phys. **86**, 5687 (1999).
[25] C. Lamberti, Surf. Sci. Rep. **53**, 1 (2004).
[26] J. Avila, C. Casado, M. C. Asensio, J. L. Pérez, M. C. Muñoz, and F. Soria, J. Vac. Sci. Technol. A **13**, 1501 (1995).
[27] A. Linkforman, D. Carré, J. Etienne, and B. Bachet, Acta Crystallogr., Sect. B: Struct. Crystallogr. Cryst. Chem. **31**, 1252 (1975).
[28] J. Rigoult, A. Rimsky, and A. Kuhn, Acta Crystallogr., Sect. B: Struct. Crystallogr. Cryst. Chem. **36**, 916 (1980).
[29] J. Pellicer-Porres, A. Segura, V. Muñoz, and A. San Miguel, Phys. Rev. B **60**, 3757 (1999).
[30] A. L. Ankudinov, B. Ravel, J. J. Rehr, and S. D. Conradson, Phys. Rev. B **58**, 7565 (1998).
[31] A. L. Ankudinov, J. J. Rehr, J. J. Low, and S. R. Bare, J. Chem. Phys. **116**, 1911 (2002).
[32] A. L. Ankudinov, J. J. Rehr, J. J. Low, and S. R. Bare, Top. Catal. **18**, 3 (2002).
[33] J. Pellicer-Porres, Ch. Ferrer-Roca, A. Segura, L. Jacquamet, and A. Chevy, Semicond. Sci. Technol. **17**, 1023 (2002).
[34] S. Tanuma, C. J. Powell, and D. R. Penn, Surf. Interface Anal. **17**, 911 (1991).
[35] M. Piacentini, E. Doni, R. Girlanda, B. Grasso, and A. Balzarotti, Nuovo Cimento Soc. Ital. Fis., B **54**, 269 (1979).
[36] S. Doniach and M. Šunjić, J. Phys. C **3**, 285 (1970).
[37] C. D. Wagner, J. Vac. Sci. Technol. **15**, 518 (1978).
[38] E. A. Albanesi, S. J. Sferco, I. Lefebvre, G. Allan, and G. Hollinger, Phys. Rev. B **46**, 13260 (1992).
[39] J. F. Sánchez-Royo, A. Segura, J. Pellicer-Porres, J. Avila, M. C. Asensio, and A. Chevy (unpublished).
[40] P. Gomes da Costa, R. G. Dandrea, R. F. Wallis, and M. Balkanski, Phys. Rev. B **48**, 14135 (1993).
[41] F. J. Manjón, D. Errandonea, A. Segura, V. Muñoz, G. Tobías, P. Ordejón, and E. Canadell, Phys. Rev. B **63**, 125330 (2001).
[42] S. Hüfner, *Photoelectron Spectroscopy*, Vol. 82 of Springer Series in Solid-State Sciences (Springer-Verlag, Berlin, 1995).
[43] K. E. Miyano, R. Cao, T. Kendelewicz, A. K. Wahi, I. Lindau, and W. E. Spicer, Phys. Rev. B **41**, 1076 (1990).
[44] T. C. G. Reusch, M. Wenderoth, L. Winking, N. Quaas, and R. G. Ulbrich, Phys. Rev. Lett. **93**, 206801 (2004).
[45] S. M. Sze, *Physics of Semiconductor Devices* (Wiley, New York, 1981).
[46] N. Kuroda and Y. Nishima, Solid State Commun. **34**, 481 (1980). In this work, authors report values of the InSe parallel ($\epsilon_{\parallel}$) and perpendicular ($\epsilon_{\perp}$) dielectric constant of $\epsilon_{\parallel}=7.8$ and $\epsilon_{\perp}=10.9$, which gives an InSe dielectric constant of $\epsilon=\sqrt[3]{\epsilon_{\perp}\epsilon_{\parallel}^{2}}=8.7$.
[47] Ch. Ferrer-Roca, A. Segura, M. V. Andrés, J. Pellicer, and V. Muñoz, Phys. Rev. B **55**, 6981 (1997).